Human Molecular Genetics, 2018, Vol. 27, No. 2 239–253

doi: 10.1093/hmg/ddx394
Advance Access Publication Date: 7 November 2017
Original Article

ORIGINAL ARTICLE

HACE1 is essential for astrocyte mitochondrial function and influences Huntington disease phenotypes *in vivo*

Dagmar E. Ehrnhoefer[†,¶], Amber L. Southwell[‡,¶], Meenalochani Sivasubramanian, Xiaofan Qiu, Erika B. Villanueva, Yuanyun Xie, Sabine Waltl, Lisa Anderson, Anita Fazeli[‡], Lorenzo Casal, Boguslaw Felczak, Michelle Tsang and Michael R. Hayden*

Department of Medical Genetics, Centre for Molecular Medicine and Therapeutics (CMMT), CFRI, University of British Columbia, Vancouver, BC V5Z 4H4, Canada

*To whom correspondence should be addressed. Tel: +1 6048753535; Fax: +1 6048753819; Email: mrh@cmmt.ubc.ca

Abstract

Oxidative stress is a prominent feature of Huntington disease (HD), and we have shown previously that reduced levels of hace1 (HECT domain and Ankyrin repeat containing E3 ubiquitin protein ligase 1) in patient striatum may contribute to the pathogenesis of HD. Hace1 promotes the stability of Nrf2 and thus plays an important role in antioxidant response mechanisms, which are dysfunctional in HD. Moreover, hace1 overexpression mitigates mutant huntingtin (mHTT)-induced oxidative stress *in vitro* through promotion of the Nrf2 antioxidant response. Here, we show that the genetic ablation of hace1 in the YAC128 mouse model of HD accelerates motor deficits and exacerbates cognitive and psychiatric phenotypes *in vivo*. We find that both the expression of mHTT and the ablation of hace1 alone are sufficient to cause deficits in astrocytic mitochondrial respiration. We confirm the crucial role of hace1 in astrocytes *in vivo*, since its ablation is sufficient to cause dramatic astrogliosis in wild-type FVB/N mice. Astrogliosis is not observed in the presence of mHTT but a strong dysregulation in the expression of astrocytic markers in HACE1$^{-/-}$ x YAC128 striatum suggests an additive effect of mHTT expression and hace1 loss on this cell type. HACE1$^{-/-}$ x YAC128 mice and primary cells derived from these animals therefore provide model systems that will allow for the further dissection of Nrf2 pathways and astrocyte dysfunction in the context of HD.

Introduction

The complex pathogenesis of Huntington disease (HD) has been linked to defects in a large variety of critical cellular pathways, including mitochondrial function and oxidative stress (1,2). Mutant huntingtin (mHTT) expressing neurons are more vulnerable to stressors such as reactive oxygen species (ROS) or excitotoxic stimuli leading to aberrant Ca^{2+} signaling (1,3–5). Furthermore, the selective loss of medium-spiny neurons in the striatum, which is characteristic of HD, can be mimicked by the systemic application of mitochondrial toxins such as 3-nitropropionic acid (3NP) or malonate (2,6,7). mHTT can also directly interfere with mitochondrial function and dynamics as well as the mitochondrial protein import machinery and intracellular mitochondrial trafficking (8–11). Mitochondrial dysfunction is thought to contribute to the accumulation of ROS and oxidative

[†]Present address: BioMed X Innovation Center, Im Neuenheimer Feld 515, 69120 Heidelberg, Germany.
[‡]Present address: Burnett School of Biomedical Sciences, University of Central Florida, Orlando, FL 32827, USA.
[¶]The authors wish it to be known that, in their opinion, the first 2 authors should be regarded as joint First Authors.
Received: August 22, 2017. **Revised:** October 28, 2017. **Accepted:** October 31, 2017

damage, which is evident in brain as well as peripheral tissues from HD patients (12–14). Furthermore, antioxidant defense mechanisms are impaired in HD, and master regulators of these pathways such as PGC1α and Nrf2 have been proposed as potential therapeutic targets (2).

In this context, we have recently reported that the overexpression of hace1 (Homologous to the E6-AP Carboxyl Terminus domain and ankyrin repeat containing E3 ubiquitin protein ligase 1) *in vitro* mitigates oxidative stress caused by the expression of mHTT by promoting the Nrf2-dependent oxidative stress response (15). HACE1$^{-/-}$ mice show reduced expression of antioxidant genes and increased markers of oxidative stress in the brain, and hace1 protein levels are significantly reduced in postmortem striatal tissue of HD patients (15). The loss of hace1 in HD may, therefore, reduce Nrf2 activity in affected neurons and brain regions despite high levels of oxidative stress. This would lead to an inefficient antioxidant defense and progressive neuronal dysfunction and death, similar to what is observed in Alzheimer's or Parkinson's diseases (16).

The YAC128 mouse model of HD mimics an early stage of the disease, with a number of well-characterized and age-dependent progressive neurological phenotypes (17,18). Although these mice accurately model a large number of HD signs and symptoms, excessive oxidative damage comparable to what has been demonstrated in human patients has not been reported (19). In particular, the reduction in hace1 levels observed in HD patients is not recapitulated in YAC128 mice (15). In an effort to further explore the function of hace1 in HD, we created HACE1$^{-/-}$ x YAC128 mice. Although these animals show an acceleration and/or worsening of some HD-related signs compared with YAC128 mice, the ablation of hace1 in wild-type (WT) animals of the FVB/N strain also caused motor, cognitive and psychiatric deficits *in vivo* and mitochondrial defects *in vitro*. We furthermore found a significant impact of hace1 ablation on astrocytes, which is in line with the importance of this cell type for the oxidative stress response in the brain.

Results

The ablation of hace1 reduces the basal expression of specific Nrf2 target genes

We have shown previously that hace1 is required for optimal induction of Nrf2 target genes in response to oxidative stress (15). In addition, the ablation of hace1 reduces the expression of phase II protective enzymes containing antioxidant response elements (ARE) such as heme oxygenase-1 (*Hmox1*), glutathione S transferase (*GST*), glutamate-cysteine ligase (*GCLc*), Nicotinamide adenine dinucleotide phosphate quinone oxidoreductase 1 (*Nqo1*) and others under conditions of oxidative stress (15). ARE regulate both the basal and inducible activity of these genes, which constitutes an important defense mechanism against neurodegeneration (20). Astrocytes are of particular importance for the oxidative stress response *in vivo*, and recent studies have shown that Nrf2 is more active in astrocytes than in neurons (21,22). We therefore generated primary astrocyte cultures that were ∼95% pure as determined by staining for Glutamate aspartate transporter (GLAST) and subsequent fluorescence activated cell sorting (FACS) analysis (Supplementary Material, Fig. S1). Live-cell imaging with a ROS-sensitive dye revealed increased staining in astrocytes derived from YAC128, HACE1$^{-/-}$ and HACE1$^{-/-}$ x YAC128 mice at baseline (Fig. 1A, HTT genotype effect $P = 0.3891$, hace1 genotype effect $P < 0.0001$, interaction $P < 0.0001$). We then determined the expression levels of ARE-containing Nrf2 target genes to investigate the functionality of the oxidative stress response in HACE1$^{-/-}$ x YAC128 cells. Surprisingly, we found that the ablation of hace1 in astrocytes specifically reduced the expression of *Nqo1*, but not *Hmox1*, *GST* or *GCLc* (Fig. 1B–E). On the contrary, ARE-containing genes involved in glutathione metabolism (*GST* and *GClc*) were upregulated in HACE1$^{-/-}$ x YAC128 astrocytes (*GST*: HTT genotype effect $P = 0.9394$, hace1 genotype effect $P = 0.0197$, interaction $P = 0.1715$; *GCLc*: HTT genotype effect $P = 0.9373$, hace1 genotype effect $P = 0.0106$, interaction $P = 0.2060$), suggesting a compensatory pathway circumventing the need for hace1 in the regulation of these genes (Fig. 1D and E). mHTT expression in YAC128 cultures decreased *Nqo1* expression to a similar degree as seen with the ablation of hace1, with no further additive effect in HACE1$^{-/-}$ x YAC128 astrocytes (Fig. 1B) (*Nqo1*: HTT genotype effect $P = 0.0053$, hace1 genotype effect $P = 0.0008$, interaction $P = 0.0011$). *Hmox1* mRNA was also slightly decreased in YAC128 cultures (Fig. 1C), again with no discernible additive effect of hace1 ablation (*Hmox1*: HTT genotype effect $P = 0.0642$, hace1 genotype effect $P = 0.2023$, interaction $P = 0.1065$).

To confirm the functionality of Nrf2 in our cultures, we next treated astrocyte cultures with tert-butylhydroquinone (tBHQ), which stabilizes Nrf2 on the protein level and thus promotes the expression of ARE-containing genes (23). Treatment with tBHQ strongly increased the expression of *Hmox1* in astrocytes of all four genotypes, confirming that the Nrf2 response is functional in the absence of hace1 and may therefore be induced through hace1 independent pathways (Fig. 1F, tBHQ effect $P < 0.0001$, genotype effect $P = 0.4231$, interaction $P = 0.6015$).

In neurons, the ablation of hace1 again only had limited effects on the basal expression of ARE-containing genes. Although *Hmox1* levels were similarly reduced in YAC128 and HACE1$^{-/-}$ cells with no additive effect in HACE1$^{-/-}$ x YAC128 cultures (Supplementary Material, Fig. S2A, HTT genotype effect $P = 0.0002$, hace1 genotype effect $P = 0.0005$, interaction $P = 0.0934$), *Nqo1* expression was only affected in neurons derived from HACE1$^{-/-}$ x YAC128 mice (Supplementary Material, Fig. S2B, HTT genotype effect $P = 0.7066$, hace1 genotype effect $P = 0.0119$, interaction $P = 0.4429$). As in astrocytes, the expression of *Hmox1* was dramatically increased for all genotypes after treatment with tBHQ (Supplementary Material, Fig. S2C, tBHQ effect $P < 0.0001$, genotype effect $P = 0.1450$, interaction $P = 0.2109$).

Taken together, the expression of Nrf2 target genes is differentially affected by the ablation of hace1 in neurons and astrocytes, suggesting cell type-specific regulatory mechanisms in the oxidative stress response. Interestingly, the expression of mHTT alone in YAC128 cultures is sufficient to lower mRNA levels of *Hmox1* in neurons and *Nqo1* in astrocytes, even though ROS levels are elevated.

mHTT expression and loss of hace1 cause mitochondrial dysfunction

In addition to promoting ARE-mediated transcription, Nrf2 is also well-known for supporting mitochondrial function and integrity under basal as well as oxidative stress conditions. The ablation of Nrf2 impairs the activity of respiratory complex I, lowers mitochondrial membrane potential and reduces adenosine triphosphate (ATP) generation through reduced oxidative phosphorylation (24). To evaluate the impact of hace1 ablation and concomitant expression of mHTT on mitochondrial

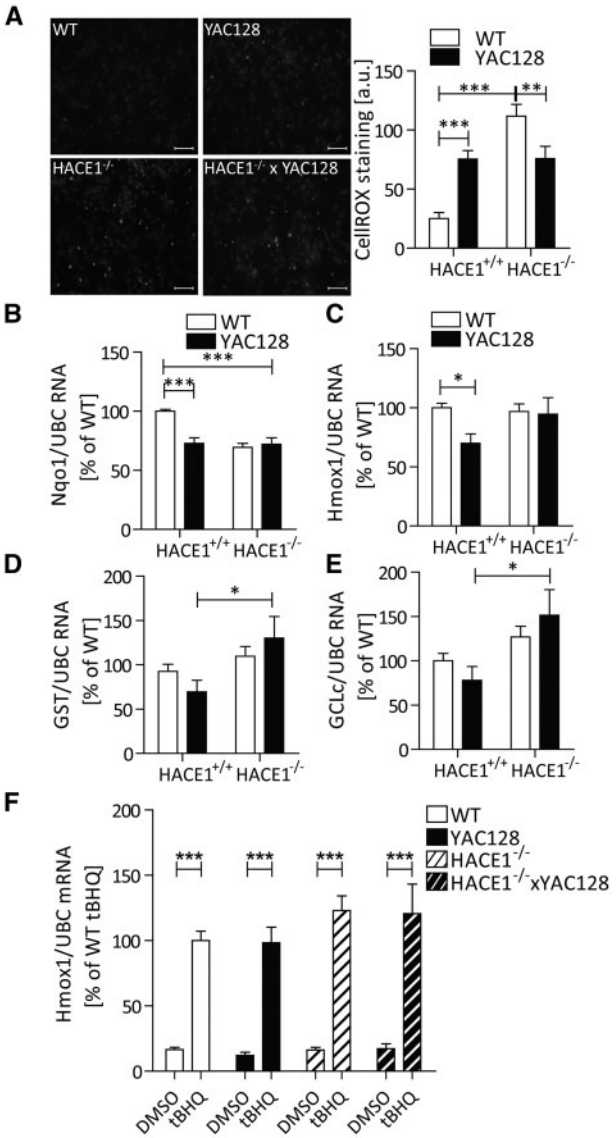

Figure 1. Loss of hace1 and mHTT expression reduce the basal expression of Nrf2 target genes. (**A**) Live imaging of primary cortical astrocytes stained with the CellROX reagent revealed increased ROS levels in YAC128, HACE1$^{-/-}$ and HACE1$^{-/-}$ x YAC12 cultures compared with WT. (**B–E**) RNA was extracted from primary cortical astrocyte cultures of WT, YAC128, HACE1$^{-/-}$ and HACE1$^{-/-}$ x YAC128 mice and the expression of *Nqo1* (B), *Hmox1* (C), *GST* (D) and *GCLc* (E) was assessed by quantitative real time polymerase chain reaction (qRT-PCR). (**F**) Primary astrocyte cultures were treated with 5 μg/ml tBHQ or Dimethyl sulfoxide (DMSO) for 24 h before RNA extraction. The expression of *Hmox1* was assessed by qRT-PCR. *Nqo1* expression is reduced by both mHTT expression and loss of hace1 alone, while *Hmox1* RNA levels are only reduced in YAC128 astrocytes. GST and GCLc RNA is upregulated in HACE1$^{-/-}$ x YAC128 compared with YAC128 astrocytes. In all samples, *Hmox1* can be transcriptionally upregulated by the Nrf2 activator tBHQ. qRT-PCR data in (B–E) were normalized to the expression of *ubiquitin c (UBC)*. All graphed data are pooled results of three independent cultures graphed with S.E.M. Statistical significance was determined by two-way analysis of variance (ANOVA) with Bonferroni *post hoc* correction. *$P < 0.05$, **$P < 0.01$, ***$P < 0.001$.

function, we performed respiratory flux experiments on astrocytes using a *Seahorse* extracellular flux analyser (25,26). The *Seahorse* instrument uses the sequential addition of oligomycin, carbonyl cyanide-p-trifluoromethoxyphenylhydrazone (FCCP) and a combination of rotenone and antimycin A coupled with continuous monitoring of the oxygen consumption rate (OCR) to determine basal respiration, ATP production, maximal respiration and proton leak of living cells and thus provides a comprehensive profile of mitochondrial function (25,26). Basal respiratory capacity equals the OCR measured by the instrument from untreated cells. After the injection of the ATP synthase inhibitor oligomycin, the OCR drops, and this difference represents the respiration required for ATP synthesis (26). Next, the uncoupling reagent FCCP is added, which dissipates the mitochondrial membrane potential ($\Delta\Psi$m) and thus unmasks the total, $\Delta\Psi$m-independent capacity of the respiratory chain (26). Lastly, the difference in OCR between basal and maximal respiration yields the spare respiratory capacity, an indicator of how close to their maximal potential mitochondria are operating at baseline (26).

Interestingly, we found that both YAC128 and HACE1$^{-/-}$ astrocytes show a dramatic impairment in all respiratory parameters measured with the exception of the oxygen consumption linked to ATP synthesis, where the deficits were more subtle (Fig. 2A–D, basal respiration: HTT genotype effect $P = 0.0131$, hace1 genotype effect $P < 0.0001$, interaction $P = 0.0067$; ATP production: HTT genotype effect $P = 0.1861$, hace1 genotype effect $P = 0.0291$, interaction $P = 0.1287$; maximal respiration: HTT genotype effect $P = 0.0127$, hace1 genotype effect $P = 0.0002$, interaction $P = 0.0046$; spare respiratory capacity: HTT genotype effect $P = 0.0029$, hace1 genotype effect $P < 0.0001$, interaction $P = 0.0046$). We did not observe an additive effect in the impairment of mitochondrial respiration in HACE1$^{-/-}$ x YAC128 cells.

Studies on Nrf2$^{-/-}$ mouse embryonic fibroblasts (MEFs) and neurons have shown that these cells have a significantly reduced basal $\Delta\Psi$m (27). When we measured $\Delta\Psi$m in our astrocyte cultures by staining active mitochondria with the dye tetramethylrhodamine (TMRE), we found a significant reduction at baseline in cells expressing mHTT, with no additional effect of hace1 ablation (Fig. 2E, HTT genotype effect $P = 0.0144$, hace1 genotype effect $P = 0.9502$, interaction $P = 0.5894$). The stepwise addition of oligomycin and FCCP did not reveal any further genotypic differences and depolarized mitochondria to a similar degree in all cultures (Fig. 2F, genotype effect $P = 0.2059$, treatment effect $P = 0.0014$, interaction $P = 0.8864$). Taken together, these data suggest that unlike Nrf2, hace1 does not play a major role in the maintenance of $\Delta\Psi$m.

mHTT expression as well as loss of hace1 impair astrocyte proliferation

Impaired mitochondrial function and decreased ATP levels affect cell proliferation (28–30), and we noticed that primary astrocytes of different genotypes seemed to consistently proliferate at different rates. We therefore decided to label actively proliferating cells in culture using BrdU. With this method, we detected fewer positive cells for YAC128, HACE1$^{-/-}$ and HACE1$^{-/-}$ x YAC128 astrocytes compared with WT (Fig. 3A), although the effect of mHTT expression alone did not reach statistical significance (HTT genotype effect $P = 0.0582$, hace1 genotype effect $P = 0.0201$, interaction $P = 0.0204$). These proliferation deficits were even more pronounced and highly significant when manual counting on consecutive days was used to determine cell numbers in parallel astrocyte cultures. Astrocytes derived from either YAC128 or HACE1$^{-/-}$ mice exhibited slower growth than WT cells, while the cell numbers for HACE1$^{-/-}$ x YAC128 astrocytes hardly increased at all over 4 days (Fig. 3B) (HTT genotype effect $P < 0.0001$, hace1

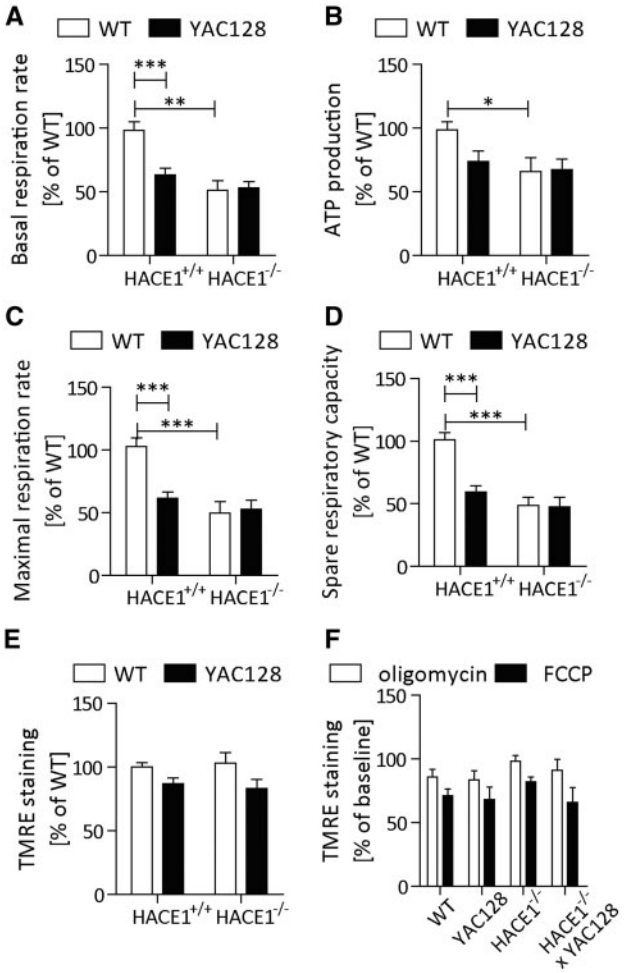

Figure 2. Loss of hace1 and mHTT expression impair astrocytic mitochondrial function. (**A–D**) Primary astrocyte cultures from WT, YAC128, HACE1$^{-/-}$ and HACE1$^{-/-}$ x YAC128 mice were grown in 96-well plates compatible with the *Seahorse* analyzer. OCRs were measured at baseline (A), after the addition of oligomycin (B) and the addition of FCCP (C). Spare respiratory capacity in (D) was calculated as the difference between maximal and basal respiration rate. mHTT expression and the ablation of HACE1 alone significantly reduce basal and maximal respiratory capacity as well as the spare respiration rate with no further additive effect in HACE1$^{-/-}$ x YAC128 cultures. OCR necessary for ATP production is only marginally reduced in HACE1$^{-/-}$ astrocytes. (**E**) and (**F**) ΔΨm was determined in primary cortical astrocytes through the quantification of TMRE staining. (E) Basal ΔΨm is significantly reduced in YAC128 and HACE1$^{-/-}$ x YAC128 astrocytes. (F) The sequential addition of oligomycin and FCCP reduces TMRE fluorescence through the dissipation of ΔΨm with no differences between cells of different genotypes. All graphed data are pooled results of independent cultures from a total of 3–7 pups per genotype graphed with S.E.M. Statistical significance was determined by two-way ANOVA with Bonferroni *post hoc* correction. $^{*}P < 0.05$, $^{**}P < 0.01$, $^{***}P < 0.001$.

genotype effect $P < 0.0001$, interaction $P = 0.0221$). These proliferation deficits are likely due to the metabolic dysfunction observed earlier, and taken together our data suggest that both the ablation of hace1 and the expression of mHTT strongly impair astrocytic mitochondrial respiration and proliferation.

Hace1 deficiency accelerates onset of motor deficits in YAC128 mice

We next decided to investigate the impact of hace1 ablation on HD-like phenotypes *in vivo*. Progressive motor deficits are a cardinal feature of HD (31) that is recapitulated in YAC128 mice (17). To assess motor performance, longitudinal accelerating rotarod and spontaneous climbing tests were performed at 2 month intervals from 2 to 12 months of age. YAC128 mice performed similarly to WT littermates in the accelerating rotarod task at 2 months of age. However, performance declined with age leading to a significantly reduced latency to fall from the rod by 4 months of age (HTT genotype effect $P < 0.0001$) (Fig. 4A), consistent with previous studies (17,32). HACE1$^{-/-}$ performed similar to WT mice, with a trend toward reduced latency to fall observed in older mice that did not reach significance by *post hoc* analysis (Fig. 4A). Similar to YAC128 mice, HACE1$^{-/-}$ x YAC128 animals showed a significant deficit at older ages. However, this group was also impaired at 2 months of age, falling from the rod significantly sooner than WT littermates (Fig. 4A), indicating an earlier onset of progressive motor deficits in YAC128 mice that lack hace1 (hace1 genotype effect $P < 0.0001$, interaction $P = 0.2857$).

In a second assessment of motor activity, YAC128 mice spent significantly less time climbing than WT littermates at 2 months of age. After 4 months of age only negligible spontaneous climbing was observed in this genotype (HTT genotype effect $P < 0.0001$) (Fig. 4B), consistent with previous findings (33,34). HACE1$^{-/-}$ mice performed similar to YAC128 mice in this task, indicating that hace1 deficiency alone can induce deficits in spontaneous climbing. HACE1$^{-/-}$ x YAC128 mice performed significantly worse than YAC128 mice at 2 months of age, confirming an acceleration of the YAC128 motor deficit by hace1 deficiency (hace1 genotype effect $P < 0.0001$, interaction $P = 0.9043$) (Fig. 4B).

Hace1 deficiency exacerbates depressive-like behavior in YAC128 mice

Depression is the most common psychiatric change associated with HD, occurring in as many as 50% of HD mutation positive individuals (31). To assess depressive-like behavior in WT, YAC128, HACE1$^{-/-}$ and HACE1$^{-/-}$ x YAC128 littermates, 12-month-old mice were subjected to forced swimming and time spent immobile was scored. In this test, YAC128 mice spent significantly more time immobile than WT mice (HTT genotype effect $P < 0.0001$) (Fig. 5A), consistent with previous reports (35,36). Although the ablation of hace1 alone did not significantly impact the time immobile in this task, HACE1$^{-/-}$ x YAC128 mice performed worse than both HACE1$^{-/-}$ and YAC128 mice (hace1 genotype effect $P = 0.0103$, interaction $P = 0.1201$) (Fig. 5A), suggesting an exacerbation of the YAC128 depressive-like phenotype by hace1 deficiency.

Hace1 deficiency may induce hypoactivity and anxiety-like behavior in WT mice

Anxiety is common in HD mutation carriers and often precedes onset of motor symptoms (31). Exploration of an elevated plus maze or a brightly lit open field was used to assess anxiety-like behavior in WT, YAC128, HACE1$^{-/-}$ and HACE1$^{-/-}$ x YAC128 littermates. Six-month-old YAC128 mice displayed anxiety-like behavior during elevated plus maze exploration, spending significantly less time in the open arms than WT littermates (HTT genotype effect $P < 0.0001$). There was no effect of hace1 loss on this phenotype (hace1 genotype effect $P = 0.1466$, interaction $P = 0.9176$) (Fig. 5B).

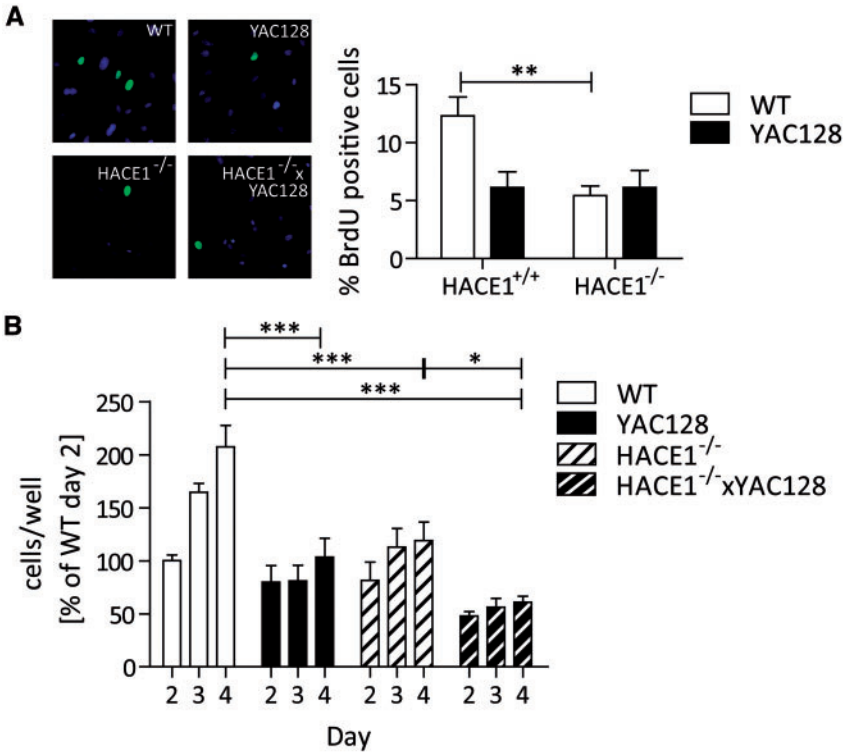

Figure 3. Loss of hace1 and mHTT expression reduce astrocyte proliferation *in vitro*. (**A**) Primary astrocyte cultures from WT, YAC128, HACE1$^{-/-}$ and HACE1$^{-/-}$ x YAC128 mice were treated with BrdU and the percentage of nuclei with positive staining was determined. Representative images are shown. (**B**) Parallel cultures of primary astrocytes were trypsinized and counted at 2–4 days after the initial seeding of equal cell numbers to determine proliferation. Both experiments demonstrate decreased proliferative capacity of YAC128, HACE1$^{-/-}$ and HACE1$^{-/-}$ x YAC128 astrocytes *in vitro*. All graphed data are pooled results of three independent cultures with S.E.M. Statistical significance was determined by two-way ANOVA with Bonferroni *post hoc* correction. *$P < 0.05$, **$P < 0.01$, ***$P < 0.001$.

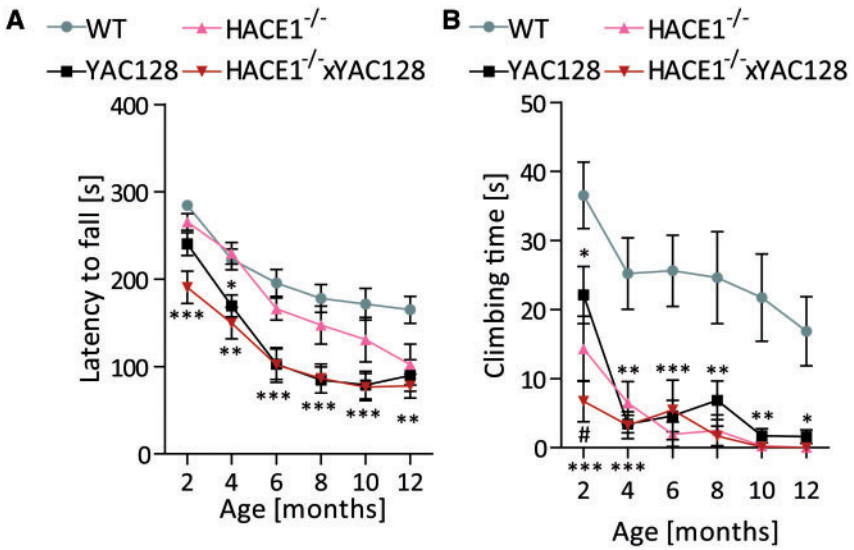

Figure 4. Loss of hace1 accelerates the onset of motor deficits in YAC128 mice. (**A**) Motor performance was evaluated in the longitudinal accelerating rotarod task. Latency to fall from the accelerating rod was scored at 2 month intervals from 2 to 12 months of age. YAC128 mice performed similarly to WT littermates at 2 months of age but displayed progressive motor deficits from 4 months of age as measured by significantly reduced latency to fall. Hace1 loss alone had no effect on motor performance as HACE1$^{-/-}$ mice performed similarly to WT mice at all ages. HACE1$^{-/-}$ x YAC128 mice displayed the earliest onset motor deficits of all experimental genotypes with significantly shorter latency to fall compared with WT littermates from 2 months of age. (**B**) Motor performance was evaluated in the longitudinal test of spontaneous climbing. YAC128, HACE1$^{-/-}$ and HACE1$^{-/-}$ x YAC128 mice all spent significantly less total time climbing during a 5 min exploration than WT littermates. HACE1$^{-/-}$ x YAC128 mice displayed a strong deficit already at 2 months of age, spending significantly less time climbing than YAC128 littermates at this early timepoint. Mean ± S.E.M. is graphed. Statistical significance was determined by two-way ANOVA with Bonferroni *post hoc* correction. *Different from WT, #different from YAC128. *$P < 0.05$, **$P < 0.01$, ***$P < 0.001$.

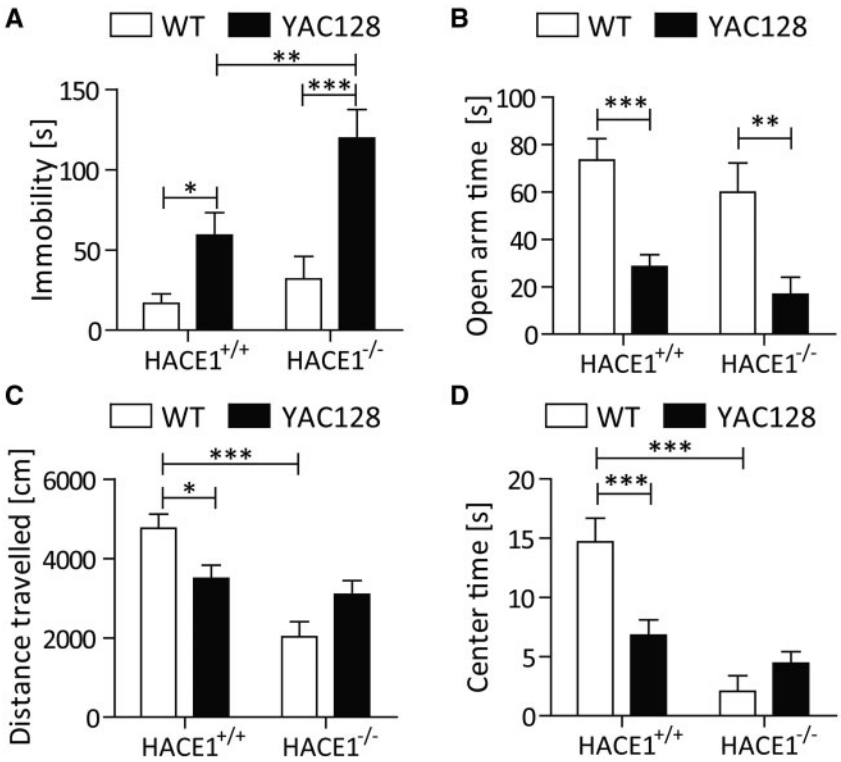

Figure 5. Loss of hace1 influences specific psychiatric phenotypes in WT and YAC128 mice. (**A**) Depressive-like behavior was evaluated by time spent immobile during forced swimming at 12 months of age. YAC128 mice displayed depressive-like behavior, spending more time immobile than WT littermates. HACE1$^{-/-}$ performed similarly to WT littermates but HACE1$^{-/-}$ x YAC128 mice spent more time immobile than HACE1$^{-/-}$ or YAC128 littermates, indicating that hace1 loss exacerbates the depressive-like behavior of YAC128 mice. (**B**) Anxiety-like behavior was evaluated by time spent in the open arms during a 5 min exploration of an elevated plus maze at 6 months of age. YAC128 mice exhibited an anxiety-like phenotype spending less time in the open arms compared with WT littermates. Hace1 loss had no effect on this behavior as HACE1$^{-/-}$ mice performed similarly to WT littermates, and HACE1$^{-/-}$ x YAC128 mice performed similarly to YAC128 littermates with no further worsening. (**C**) Exploratory activity was evaluated by total distance traveled during a 10 min exploration of a brightly lit open field at 8 months of age. YAC128 mice displayed hypoactivity with less total distance traveled than WT littermates. Hace1 loss induced hypoactivity in HTT WT mice (HACE1$^{-/-}$) but had no exacerbating effect on activity in YAC128 mice (HACE1$^{-/-}$ x YAC128). (**D**) Anxiety-like behavior was evaluated by time spent in the center of a brightly lit open field during a 10 min exploration at 8 months of age. YAC128 mice displayed anxiety-like behavior spending less time in the center of the field than WT littermates. This was not worsened by hace1 loss as HACE1$^{-/-}$ x YAC128 mice performed similarly to YAC128 mice. Conversely, hace1 loss induced anxiety-like behavior in HTT WT mice as HACE1$^{-/-}$ mice performed similarly to YAC128 mice spending less time in the center of the field than WT littermates. Mean ± S.E.M. is graphed. Statistical significance was determined by two-way ANOVA with Bonferroni *post hoc* correction. *Difference between indicated bars, *$P < 0.05$, **$P < 0.01$, ***$P < 0.001$.

At 8 months of age, when animals were exposed to the open field apparatus, YAC128 mice were hypoactive with reduced total distance traveled compared with WT mice. HACE1$^{-/-}$ x YAC128 mice traveled a similar distance as YAC128 mice, while hace1 loss alone induced hypoactivity, as HACE1$^{-/-}$ mice traveled significantly less than WT mice (HTT genotype effect $P = 0.7869$, hace1 genotype effect $P < 0.0001$, interaction $P = 0.0026$) (Fig. 5C). The quantification of time spent in the center of the open field confirmed these results: YAC128 mice spent significantly less time in the center compared with WT mice (HTT genotype effect $P = 0.0491$) (Fig. 5D), consistent with previous reports (33,34).

Both HACE1$^{-/-}$ x YAC128 and HACE1$^{-/-}$ mice displayed an anxiety-like phenotype similar to YAC128 animals (hace1 genotype effect $P < 0.0001$, interaction $P = 0.0011$) (Fig. 5D). Although the anxiety phenotype in YAC128 mice is thus not further exacerbated by the loss of hace1 in either of the two tests we performed, the ablation of hace1 alone was sufficient to induce anxious behavior in open field but not elevated plus maze exploration. However, the elevated plus maze exploration test was performed at 6 months of age, while open field exploration was performed later at 8 months of age. It is therefore possible that hace1 loss causes anxiety with a late onset, which was not yet apparent at 6 months of age.

Hace1 deficiency may exacerbate cognitive deficits in YAC128 mice

Cognitive deficits can precede onset of motor symptoms in HD (31) and in YAC128 mice (32). To evaluate the effect of hace1 loss on cognitive performance in YAC128 mice, motor learning was evaluated on the rotarod at 2 months of age and object location and recognition learning assays were performed at 4 months of age.

During the training phase with a fixed speed rotarod paradigm, YAC128 mice fell more frequently and sooner from the rod than WT mice on training days 1 and 2, respectively. This suggests a motor learning deficit, which is consistent with previous reports (32). On training day 3, YAC128 mice performed similarly to WT mice, indicating that motor performance, on the other hand, is normal at this age (Fig. 6A and B). HACE1$^{-/-}$ mice exhibited normal motor performance and motor learning, while HACE1$^{-/-}$ x YAC128 mice fell more frequently (days 1–2) and sooner (days 1–3) from the rod than WT mice. HACE1$^{-/-}$ x

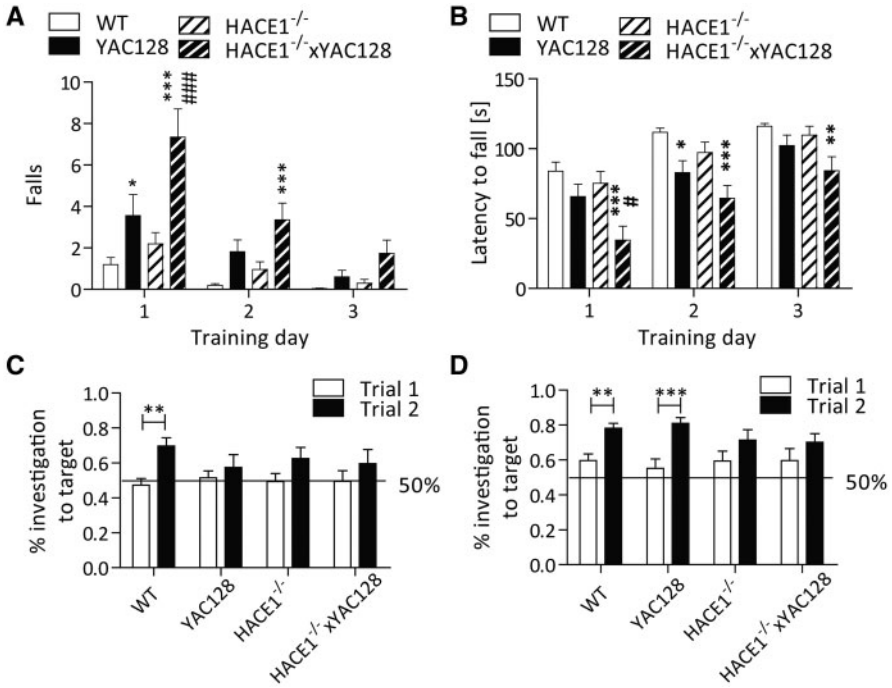

Figure 6. Loss of hace1 may exacerbate cognitive deficits in YAC128 mice. (**A** and **B**) Motor learning was assessed at 2 months of age during rotarod training. YAC128 mice exhibited impaired motor learning, falling more frequently (A) and sooner (B) from the rod than WT mice during training despite no deficit in performance during accelerating rotarod testing at this age. HACE1$^{-/-}$ mice performed similarly to WT littermates, indicating no deficits in motor learning. HACE1$^{-/-}$ x YAC128 mice fell more frequently (A) and sooner (B) from the rod than YAC128 littermates, indicating a possible exacerbation of motor learning deficits. However, these mice also exhibited significant motor deficits during accelerating rotarod testing at this age, confounding interpretation of motor learning performance. (**C** and **D**) Spatial learning and object recognition were evaluated at 4 months of age by preference for a known object in a novel location (C) or preference for a novel object (D). WT mice exhibited normal learning in both paradigms, while YAC128 mice showed no preference for a moved object, indicating a spatial learning deficit. YAC128 mice did show a preference for a novel object, indicating intact object recognition at this age. HACE1$^{-/-}$ and HACE1$^{-/-}$ x YAC128 mice failed to exhibit normal learning in either paradigm, indicating that hace1 loss is sufficient to disrupt both spatial learning and object recognition. Mean ± S.E.M. is graphed. Statistical significance was determined by two-way ANOVA with Bonferroni *post hoc* correction. For A and B, *different from WT, #different from YAC128 and for C and D, *difference between indicated bars, *$P < 0.05$, **$P < 0.01$, ***$P < 0.001$.

YAC128 mice also performed worse than YAC128 on training day 1 (Fig. 6A and B), suggesting an exacerbation of the YAC128 motor learning deficit. However, HACE1$^{-/-}$ x YAC128 mice also showed overall impaired motor performance on the rotarod at this age (Fig. 4A), which may confound the results and preclude an accurate analysis of cognitive deficits.

Therefore, we next assessed spatial learning and object recognition at 4 months of age by preference for a known object in a novel location or for a novel object, respectively. This time point was chosen because at this age YAC128 mice have impaired object location learning but intact object recognition (unpublished). Thus, it would allow detection of either an amelioration or exacerbation of cognitive deficits.

WT mice showed a preference for a known object in a novel location, spending more time investigating a moved object than one in its original position. YAC128, HACE1$^{-/-}$ and HACE1$^{-/-}$ x YAC128 mice showed no preference for investigating the moved object (Fig. 6C), suggesting that mHTT or hace1 loss are sufficient to disrupt object spatial learning at this age. Both WT and YAC128 mice showed a preference for a novel object over a known object. Neither HACE1$^{-/-}$ nor HACE1$^{-/-}$ x YAC128 mice showed a significant preference for a novel object (Fig. 6D), indicating that hace1 loss is sufficient to disrupt object recognition. Taken together, these results suggest that hace1 loss is sufficient to induce cognitive deficits and may accelerate onset or exacerbate severity of cognitive deficits in YAC128 mice.

Hace1 deficiency increases forebrain size and causes astrogliosis in WT but not YAC128 mice

Forebrain-specific atrophy and reduced striatal volume due to the loss of medium-spiny neurons are neuropathological features of HD that are recapitulated in YAC128 mice (37,38). These phenotypes are particularly pronounced on the FVB/N strain, which may be due to the sensitivity to excitotoxicity of this mouse strain (39,40).

At 3 months of age, YAC128 mice do not yet exhibit forebrain weight loss (HTT genotype effect $P = 0.2036$). However, the ablation of hace1 alone increased forebrain weight (hace1 genotype effect $P = 0.0352$, interaction $P = 0.2727$), although this difference failed to reach *post hoc* significance (Supplementary Material, Fig. S3A). As expected, YAC128 mice had significantly reduced forebrain weight compared with WT littermates by 12 months of age (HTT genotype effect $P < 0.0001$), while the forebrain weight of HACE1$^{-/-}$ animals showed a dramatic increase compared with WT (Fig. 7A). Interestingly, HACE1$^{-/-}$ x YAC128 mice exhibited similar forebrain weight loss as YAC128 (hace1 genotype effect $P = 0.0015$, interaction $P = 0.0084$) (Fig. 7A).

This bimodal effect of hace1 ablation that is dependent on the presence or absence of mHTT was mirrored by striatal and cortical volume measurements: in agreement with published data, a trend toward reduced striatal volume was observed in 3-month-old YAC128 mice (HTT genotype effect $P = 0.0007$) (Supplementary Material, Fig. S3B), and a significant reduction

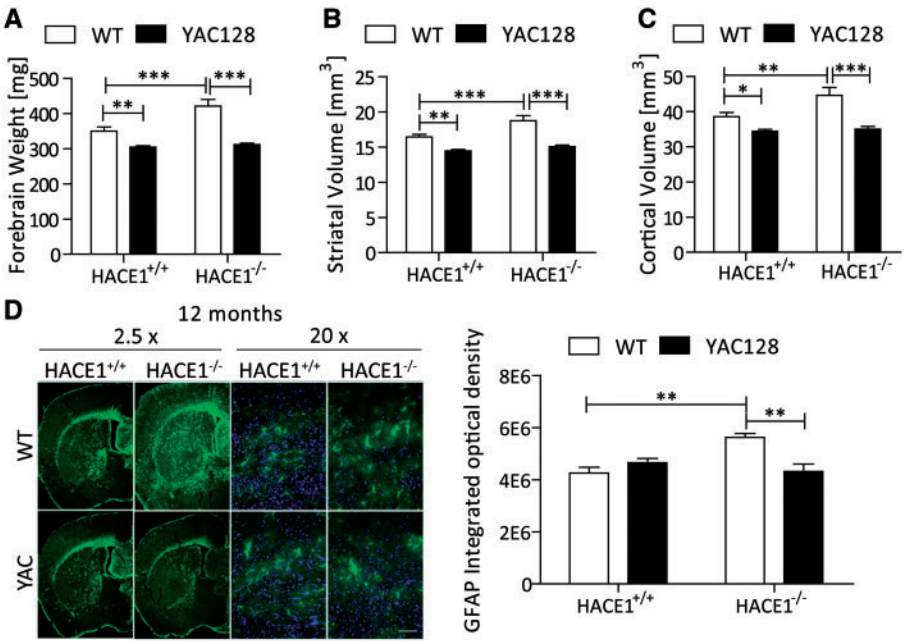

Figure 7. The loss of hace1 causes astrogliosis in WT but not YAC128 mice. (**A–C**) Forebrain specific atrophy was evaluated at 12 months of age by forebrain weight, striatal and cortical volume. Both YAC128 and HACE1$^{-/-}$ x YAC128 (A) forebrains, (B) striata and (C) cortices were significantly smaller than WT littermates at this time-point, demonstrating forebrain atrophy that is not altered by hace1 loss. Conversely, HACE1$^{-/-}$ (A) forebrains (B) striata and (C) cortices were significantly larger than those from WT littermates. (**D**) GFAP immunostaining at 12 months of age demonstrated excessive reactive astrogliosis in HACE1$^{-/-}$ brains, suggesting that HACE1 loss promotes reactive astrogliosis that is prevented by overexpression of HTT. Mean ± S.E.M. is graphed. Statistical significance was determined by two-way ANOVA with Bonferroni *post hoc* correction. *Difference between indicated bars, *$P < 0.05$, **$P < 0.01$, ***$P < 0.001$.

in striatal and cortical volume was seen at 12 months of age (Fig. 7B and C, striatum: HTT genotype effect $P < 0.0001$, cortex: HTT genotype effect $P < 0.0001$). Hace1 loss did not affect striatal volume in YAC128 mice but increased striatal volume at both 3 and 12 months and cortical volume at 12 months of age on a WT background (Supplementary Material, Fig. S3B, Fig. 7B and C, striatum: 3 mo hace1 genotype effect $P = 0.0224$, interaction $P = 0.1038$, 12 mo hace1 genotype effect $P = 0.0016$, interaction $P = 0.0558$, cortex: 12 mo hace1 genotype effect $P = 0.0153$, interaction $P = 0.0452$). These phenotypes are reminiscent of a sporadic seizure disorder prominent in FVB/N mice, which can lead to reactive astrogliosis and enlarged forebrains (41–43).

Consistent with this phenomenon, we noted mild striatal astrogliosis in 3-month-old HACE1$^{-/-}$ mice that was not present in WT, YAC128 mice and HACE1$^{-/-}$ x YAC128 animals (Supplementary Material, Fig. S3C). At 12 months of age, striatal glial fibrillary acidic protein (GFAP) immunoreactivity was higher in all four genotypes than at 3 months, consistent with a normal age-dependent increase in GFAP expression (44,45). However, striatal GFAP staining in 12-month-old HACE1$^{-/-}$ brains was significantly more intense and dense than in WT brains (hace1 genotype effect $P = 0.0384$), indicating widespread reactive astrogliosis. This effect was not seen in YAC128 or HACE1$^{-/-}$ x YAC128 brains (Fig. 7D) (HTT genotype effect $P = 0.0630$; interaction $P = 0.0036$).

Hace1 deficiency differentially alters the expression of astrocyte markers in WT and YAC128 striatum

To analyze the differences in reactive astrocytes between HACE1$^{-/-}$ and HACE1$^{-/-}$ x YAC128 mice in more detail, we used quantitative RT-PCR analysis to determine the expression of the astrocytic marker genes *GFAP*, *S100β* and *Slc1a3* (Glast). In line with the absence of astrogliosis in HACE1$^{-/-}$ x YAC128 animals, we detected that the presence of mHTT led to a significant decrease in striatal GFAP expression (Fig. 8A, HTT genotype effect $P = 0.0009$, hace1 genotype effect $P = 0.09977$, interaction $P = 0.4142$). Interestingly, HACE1$^{-/-}$ x YAC128 mice showed a strong upregulation of *S100β* compared with their HACE1$^{-/-}$ littermates (Fig. 8B, HTT genotype effect $P = 0.0093$, hace1 genotype effect $P = 0.3683$, interaction $P = 0.0059$). The expression of *Slc1a3* showed no statistically significant differences between experimental genotypes, suggesting that this marker is not altered by astrogliosis (Fig. 8C, HTT genotype effect $P = 0.7494$, hace1 genotype effect $P = 0.1038$, interaction $P = 0.0140$).

Taken together, these results suggest that the loss of hace1 increases the natural susceptibility of FVB/N WT mice to astrogliosis and cerebral hypertrophy, while the overexpression of mHTT in YAC128 mice prevents this pathology. These differences are reflected by opposing expression patterns of the reactive astrocyte markers *GFAP* and *S100β*. Since astrogliosis phenotypes have been reported in Nrf2$^{-/-}$ mice (46), the HACE1$^{-/-}$ phenotype may be due to reduced Nrf2 activity.

Discussion

Oxidative stress and mitochondrial dysfunction are well-described features of HD and have been observed in a variety of cells and tissues directly derived from patients (4,12–14,47). mHTT itself can localize to the mitochondria where it causes defects in mitochondrial fission dynamics and mitochondrial protein import (11,48). In addition, there is evidence for the impairment of PGC1α, a master regulator of mitochondrial function, in HD (49–55). Together with Nrf2, PGC1α regulates the expression of nuclear-encoded mitochondrial genes, and it also contributes to the expression of ARE-containing phase II

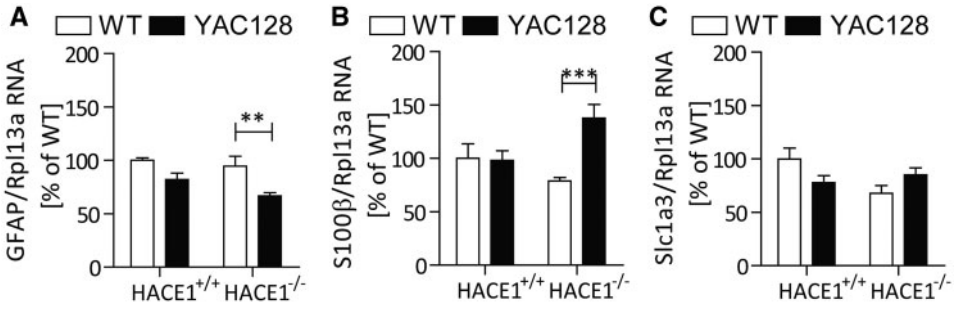

Figure 8. The loss of hace1 causes a differential expression pattern of astrocytic markers in WT and YAC128 mice. (**A–C**) RNA levels of *GFAP* (A), *S100β* (B) or *Slc1a3* (C) were determined by qPCR in striatal tissue of 6-month-old animals. (A) mHTT expression reduced *GFAP* levels, and this effect was particularly pronounced in the absence of hace1. (B) *S100β* expression, on the contrary, was significantly increased in HACE1$^{-/-}$ x YAC128 striatum, suggesting that the activation status of astrocytes in these brains differs from HACE1$^{-/-}$ samples. (C) No significant differences in the expression of the astrocyte marker *Slc1a3* were observed in all four experimental genotypes. Mean ± S.E.M. is graphed. Statistical significance was determined by two-way ANOVA with Bonferroni *post hoc* correction. *Difference between indicated bars, *$P < 0.05$, **$P < 0.01$, ***$P < 0.001$.

detoxifying enzymes (55,56). For these reasons, the activation of both PGC1α and Nrf2 have been proposed as therapeutic strategies to counteract oxidative stress and mitochondrial dysfunction in HD. Nrf2 activators have shown promising results in HD mouse models (57,58) but most of these studies were performed in models expressing only a short N-terminal fragment of mHTT (R6/2 or N171–82Q) with only modest benefits seen in YAC128 mice that express full-length mHTT (57). Moreover, the agents used are not potent Nrf2 agonists and have activity against numerous other targets, which may have mitigated the positive effects. This is consistent with a study reporting no oxidative damage in brain tissues from YAC128 mice up to 12 months of age (19). Nrf2 dysfunction in HD patients may be in part due to reduced levels of hace1 (15), and to evaluate the impact of hace1 loss on the well-characterized HD-like phenotypes of the YAC128 model, we generated HACE1$^{-/-}$ x YAC128 mice.

Although increased neuronal Nrf2 activity is protective in the R6/2 and YAC128 mouse models of HD (57), astrocytic Nrf2 activity specifically protects from 3NP and malonate-induced toxicity (59). Astrocytes are important mediators of protection from oxidative stress, and the constitutive ablation of Nrf2, in particular, leads to an astrogliosis phenotype *in vivo* (46). The contribution of astrocytes to HD pathology is not well-studied but there is evidence that the expression of mHTT in astrocytes impairs neuronal energy metabolism, possibly through increased oxidative stress (60). Astrocytes from BACHD mice expressing full-length mHTT exhibit increased glutamate release *in vitro*, which could contribute to excitotoxicity and downstream oxidative stress in neurons (61). Furthermore, a recent study shows that the expression of mHTT in glia is sufficient to cause HD-like phenotypes in mice, suggesting that glial dysfunction has a significant impact on neuronal health and the pathogenesis of HD (62).

Here, for the first time, we demonstrate astrocytic phenotypes in primary cultures derived from YAC128 mice, with significant deficits in mitochondrial respiration parameters and ΔΨm as well as reduced astrocyte proliferation rates *in vitro*. Combined with reduced Nrf2 function in HACE1$^{-/-}$ x YAC128 mice, a vicious cycle of oxidative stress and mitochondrial dysfunction may therefore be exacerbated. The changes observed in the expression of *Hmox1* and *Nqo1* in YAC128 neurons and astrocytes furthermore show that subtle alterations in the Nrf2 pathway as well as increased ROS are already present at baseline in primary astrocytes from this mouse model. These readouts should be useful to assess the impact of experimental therapeutics targeting the oxidative stress response and mitochondrial dysfunction.

We show here that the lack of hace1 causes astrogliosis *in vivo*, similar to the ablation of Nrf2 (46). This should lead to the release of pro-inflammatory factors such as NO, which is known to inhibit neuronal respiration, cause glutamate release and finally excitotoxic neuronal death (63). This phenotype may be exacerbated on the FVB/N mouse strain, which is known to be susceptible to spontaneous seizures and accompanying astrogliosis (42,43) as well as excitotoxicity (40,64). Since we back-crossed HACE1$^{-/-}$ mice to the FVB/N background for the purpose of this study, it may explain why this phenotype was not reported in the previous characterizations of HACE1$^{-/-}$ mice on a different background strain (15,65).

Interestingly, the expression of mHTT in HACE1$^{-/-}$ x YAC128 mice dramatically reduces astrogliosis and accompanying alterations in brain weight seen in their HACE1$^{-/-}$ littermates (Fig. 7). Furthermore, HACE1$^{-/-}$ x YAC128 striata show reduced expression of *GFAP* paralleled by an increase in *S100β* compared with their HACE1$^{-/-}$ littermates (Fig. 8). Such different transcriptional responses to astrocyte dysfunction may underlie the striking difference in astrogliosis observed by neuropathological methods.

A neuroprotective role for WT HTT has been established following excitotoxic stimuli both *in vitro* and *in vivo* (66). Even the expression of mHTT can be protective in these paradigms, provided that the mHTT protein contains protective posttranslational modifications (resistance to cleavage at D586 and/or phosphorylation at S421) (67,68). Furthermore, mHTT can substitute for the essential function of WT HTT during development, suggesting that it retains some of its normal functionality even in the presence of the HD mutation (69). Although no data is available on the function of WT HTT in astrocytes, it is possible that increased levels of total HTT caused by the expression of the mHTT transgene protects HACE1$^{-/-}$ x YAC128 animals from the astrogliosis phenotype.

Although the onset of astrogliosis in HACE1$^{-/-}$ mice was observed at 3 months of age and obviates the assessment of HD-like neuropathological phenotypes, there is a clear additive effect of mHTT expression and hace1 ablation on the onset of motor deficits at 2 months of age. In addition, performance in the forced swim test for depression was significantly worsened in HACE1$^{-/-}$ x YAC128 mice but not impacted by HACE1$^{-/-}$ alone at 12 months of age, suggesting that some behavioral phenotypes are not impacted by astrogliosis and are exacerbated in HACE1$^{-/-}$ x YAC128 compared with YAC128 mice.

In summary, our study shows that the loss of hace1 impacts HD-like phenotypes in the YAC128 mouse model and reduced levels of hace1 in HD patients may thus contribute to the disease. We furthermore describe mitochondrial deficits as well as reduced expression of Nrf2 target genes in primary cultures derived from YAC128 mice that further contribute to the characterization of this HD mouse model.

Materials and Methods

Mice and breeding

Mice were maintained under a 12 h light:12 h dark cycle in a clean facility and given free access to food and water. Experiments were performed with the approval of the animal care committee of the University of British Columbia. HACE1$^{-/-}$ mice on a mixed 129/Ola and C57BL/6 background (65) were backcrossed 10 generations to FVB/N by intercrossing male hace1$^{+/-}$ and female FVB/N mice. Mice were genotyped using Promega GoTaq green master mix, a common forward primer (hace1_F: 5′ TGG CTG CTA CCC CAA GTT CC 3′) and WT (500 bp product) or KO (300 bp product) reverse primer (WT_R: 5′ TTC CCC ATA GCT GCC GCA AG 3′, KO_R: 5′ AAG GGC CAG CTC ATT CCT CC 3′) with the following PCR settings: 94 °C 3 min, 35 × (94 °C 30 s, 60 °C 30 s, 72 °C 30 s), 72 °C 7 min. Hace1$^{+/-}$ females were then intercrossed with YAC128 (17) males, which express transgenic full-length human mHTT. The YAC128 transgene was genotyped as previously described (70) and the hace1 genotyping was done as earlier. This first cross produced hace1$^{+/-}$ x YAC128 mice, which were intercrossed with *hace1*$^{+/-}$ mice to yield the four genotypes at study; WT, YAC128, HACE1$^{-/-}$ and HACE1$^{-/-}$ x YAC128, as littermates. All *hace1*$^{+/-}$ mice generated from these crosses were sacrificed. Three cohorts of mice with roughly even sex and genotype distribution were used for 12 month behavioral and neuropathological assessment (total $N = 25$ WT, 22 YAC128, 18 HACE1$^{-/-}$ and 19 HACE1$^{-/-}$ x YAC128) and 1 cohort of mice with roughly even sex distribution was used for 3 month neuropathological assessment ($N = 9$ WT, 11 YAC128, 11 HACE1$^{-/-}$ and 11 HACE1$^{-/-}$ x YAC128). All mice at the 3 month time point were included in the assessment. The numbers per genotype of mice assessed at each time point in the 12 month longitudinal study are given in Supplementary Material, Table S1.

Primary neuronal and astrocyte cultures

Embryos from timed-pregnant females were collected on day 15.5–16.5 of gestation. Brains were removed and transferred to Hibernate E (Invitrogen) for up to 24 h, during which time samples from the remaining embryonic tissues were genotyped (71). Cortices were microdissected in ice-cold Hank's balanced salt solution (HBSS+; Gibco), then diced and pooled for each genotype.

For neuronal cultures, cells were dissociated with 0.05% trypsin-Ethylenediaminetetraacetic acid (EDTA) (Gibco), followed by neutralization with 10% fetal calf serum in neuro basal medium (NBM+) and DNase I treatment (153 U/ml). Tissue was triturated with a pipette five to six times. Cells were plated on poly-D-lysine coated 6-well plates with 2 ml of Neurobasal media (Gibco), B27 (Gibco), 100 U/ml penicillin-streptomycin (PS) (Gibco), 0.5 mM L-glutamine and maintained at 37 °C, 5% CO_2 with humidity. Cells were fed with 200 ml fresh medium every fifth day. On days 9–11 in culture, cells were treated with 5 μg/μl tBHQ for 24 h if necessary and harvested by scraping. Cell pellets were washed in cold phosphate buffered saline (PBS) and stored at −80 °C until further processing.

For astrocyte cultures, mouse pups at postnatal days 0–2 were sacrificed, brains were removed and stored in Hibernate E (Invitrogen) and a piece of non-central nervous system (CNS) tissue was kept for genotyping as described earlier. Cortical tissue was minced and cells were dissociated with 0.05% trypsin-EDTA (Gibco), followed by neutralization with 20% fetal calf serum in Dulbecco's modified Eagle medium (DMEM)/F12 medium (Gibco). Tissue was triturated with a pipette five to six times, and subjected to DNase I treatment (153 U/ml). Cells were plated on uncoated plates in high-glucose DMEM (Gibco) with 10% fetal calf serum, 100 U/ml PS (Gibco), 0.5 mM L-glutamine and maintained at 37 °C, 5% CO_2 with humidity. Medium was exchanged after 24 h and then every 7 days. Cells were passaged when confluent and used for experiments at passages 2–4.

Purification of astrocytes

Astrocytes were purified from the mixed glial cultures by shaking the flasks at 180rpm. The media containing the microglia and oligodendrocytes were discarded and the adherent astrocytes were split and reseeded for various experiments. The purity of the astrocytes was further confirmed using flow cytometry using GLAST antibody (Miltenyi biotech) following the manufacturer's protocol. Briefly, around 10^6 cells were centrifuged at 300*g* for 10 min. The supernatant was completely removed and the cells were resuspended in 100 μl of buffer (PBS + 0.5% bovine serum albumin [BSA]). Ten microliters of the Anti-GLAST (ACSA-1) antibody was added and incubated for 10 min in the dark (at 4 °C). After incubation, the cells were washed with buffer and centrifuged at 300*g* for 10 min. The cell pellet was resuspended in a suitable amount of buffer for analysis by flow cytometry.

RNA extraction and qRT-PCR

RNA was extracted from cultured neurons, astrocytes or striatal tissue using the PureLink mini RNA extraction kit (Life Technologies). RNA was treated with DNase I (Invitrogen) and 500 ng of RNA were reverse transcribed using SuperScript III (Invitrogen) and oligo-dT primers according to manufacturer's instructions to generate cDNA for qRT-PCR. The PCR was run with SYBR Green Power master mix (Applied Biosystems) on the ABI Prism 7500 Sequence Detection System.

Each sample was run in triplicate. Relative gene expression was determined by using the $\Delta\Delta C_T$ method, normalizing to *Rpl13a* or *UBC* mRNA levels. The following primers were used:

Nqo1 forward: 5′- AGGATGGGAGGTACTCGAATC -3′
Nqo1 reverse: 5′- TGCTAGAGATGACTCGGAAGG -3′
Hmox1 forward: 5′- AGGTACACATCCAAGCCGAGA -3′
Hmox1 reverse: 5′- CATCACCAGCTTAAAGCCTTCT -3′
GClc forward: 5′- GGCGATGTTCTTGAGACTCTGC -3′
GCLc reverse: 5′- TTCCTTCGATCATGTAACTCCCATA -3′
GST forward: 5′- CCCCTTTCCCTCTGCTGAAG -3′
GST reverse: 5′- TGCAGCTTCACTGAATCTTGAAAG -3′
GFAP forward: 5′- AACCGCATCACCATTCCTGT -3′
GFAP reverse: 5′- TAATGACCTCACCATCCCGCA -3′
S100β forward: 5′- CTGGAGAAGGCCATGGTTGC -3′
S100β reverse: 5′- CTCCAGGAAGTGAGAGAGCT -3′
Slc1a3 forward: 5′- CGCGGTGATAATGTGGTATGC -3′
Slc1a3 reverse: 5′- TGTCACGGTGTACATGGCAA -3′
Rpl13a forward: 5′- GGAGGAGAAACGGAAGGAAAAG -3′

Rpl13a reverse: 5′- CCGTAACCTCAAGATCTGCTTCTT -3′
UBC forward: 5′- AGCCCAGTGTTACCACCAAG -3′
UBC reverse: 5′- ACCCAAGAACAAGCACAAGG -3′

Metabolic flux analysis

Primary astrocytes were cultured on Seahorse XFe-96 (Seahorse BioSciences, Billerica, MA) plates at a density of 20 000 cells per well. On the day of analysis, media was changed to assay medium, pH 7.4, supplemented with 25 mM glucose and/or 1 mM pyruvate and incubated at 37 °C in a non-CO_2 incubator for 1 h. Using the Seahorse XFe96 (Seahorse BioSciences) metabolic analyzer, three baseline measurements of OCR were sampled prior to sequential injection of mitochondrial inhibitors. Three metabolic parameters were sampled following addition of each mitochondrial inhibitor prior to injection of the subsequent inhibitors. The mitochondrial inhibitors used were oligomycin (2 μM), FCCP [carbonyl cyanide 4-(trifluoromethoxy)-phenylhydrazone] (1 μM) and rotenone (0.5 μM). OCR was automatically calculated and recorded by the Seahorse software. After the assays, protein level was determined with the DC protein assay (Bio-Rad) for each well to confirm equal cell density. The protein concentration in each well was used for normalizing the data.

Measurement of mitochondrial membrane potential using TMRE

Astrocytes were cultured on a 96-well plate at a density of 20 000 cells per well. Cells were loaded with 25 nM TMRE methyl ester for 15 min at room temperature in HBSS (156 mM NaCl, 3 mM KCl, 2 mM $MgSO_4$, 1.25 mM KH_2PO_4, 2 mM $CaCl_2$, 10 mM glucose and 10 mM 4-(2-hydroxyethyl)-1-piperazineethanesulfonic acid (HEPES), pH adjusted to 7.35), and the dye was present during the experiment. TMRE fluorescence was measured using a plate reader (TMRE: Ex/Em = 549/575 nm): baseline fluorescence measurement, followed by fluorescence intensities after the sequential addition of oligomycin (3 μM) and FCCP (2 μM).

ROS assay

Oxidative stress was measured using CellROX green reagent (Life Technologies). Cells were treated with 5 μM Cell Rox Green reagent in complete medium. Following 30 min incubation, the cells were washed with PBS and imaged live on a Zeiss AXIOvert inverted microscope using a 40× objective using the same exposure settings for all samples. In total, 16–21 images were taken randomly for each genotype, and fluorescence intensity was determined as mean optical density for each image using ImageJ software.

BrdU staining

Astrocytes were cultured on coverslips and treated with 10 μM BrdU for 3 h in the incubator. Cells were then fixed with 4% paraformaldehyde (PFA) in PBS for 30 min at room temperature, permeabilized with 0.1% Triton in PBS and incubated with 1M HCl for 10 min on ice, followed by 10 min of 2M HCl at room temperature. Samples were neutralized using phosphate/citric acid buffer (182 mM Na_2HPO_4, 9 mM citric acid, pH 7.4), washed with PBS-T and incubated at 4 °C over night with anti-BrdU antibody (1:500, Santa Cruz Biotech sc-56258). Coverslips were developed with anti-rat secondary antibody coupled to Alexa 488 (Life Technologies) and mounted in 4′,6-diamidino-2-phenylindole (DAPI)-containing mounting medium (Life Technologies). Cells were imaged on a confocal microscope, a total of 80–100 cells per genotype from three independent cultures were imaged. BrdU-stained nuclei were counted using Image J software.

Cell counts for proliferation assay

Astrocytes were seeded into 6-well plates, and 2, 3 or 4 days after seeding, each single well was trypsinized and viable cells (negative for Trypan blue staining, a minimum of 50 viable cells per sample) were manually counted in a Neubauer chamber under the microscope. For each well, the number of viable cells per well was calculated. Three independent cultures with three technical replicates each were analyzed.

Behavior testing

Mice were weighed and tested on an accelerating rotarod longitudinally every 2 months from 2 to 12 months of age as described previously (72). Briefly, 2-month-old mice were trained over 3120 s trials per day for 3 days on an 18rpm fixed speed rotarod. Mice that fell were returned immediately to the rod. Mean latency to the first fall and mean falls for the three trials were scored. Mice were tested over 3300 s trials on an accelerating rotarod (5–40rpm), and mean latency to fall for the three trials was scored.

Exploration of an elevated plus maze as previously described (72) was used to evaluate anxiety-like behavior at 6 months of age. Briefly, mice were placed in the center of an elevated plus maze, and exploration was recorded during a 5 min trial by a ceiling-mounted video camera. Time spent in the open arms was scored by Ethovision XT 7 animal tracking software (Noldus) as a measure of anxiety.

Open field exploration for evaluation of anxiety-like behavior and object learning for evaluation of spatial learning and object recognition were performed as previously described (72) at 4 and 8 months of age. Briefly, mice were placed in a 50 × 50 cm open top box under bright lighting and exploration was recorded during a 10 min trial by a ceiling-mounted video camera. Distance traveled and time spent in the center of the field were scored as measures of activity and anxiety, respectively, using Ethovision XT 7. After a 5 min intertrial interval (ITI), mice were returned to the box, now containing two objects in the upper corners. After a 5 min exploration, mice were given a 5 min ITI during which the right hand object was moved to the lower corner. Mice were then given another 5 min exploration. The proportion of investigations to the target object on the right was scored using Ethovision XT 7 as a measure of spatial learning. On the following day, mice were returned to the box for a 5 min acclimation, given a 5 min ITI and then allowed to explore the box for 5 min with the same two objects now back in their original positions. After a 5 min ITI, the object on the right was replaced with a novel object and the mice were given another 5 min exploration. The proportion of investigations to the target objet on the right was scored using Ethovision XT 7 as a measure of object recognition. Data for any mouse that failed to investigate both objects were excluded.

A modified Porsolt forced swim test for evaluation of depressive-like behavior was performed as previously described (35) at 12 months of age. Briefly, mice were placed in transparent cylinders filled with room temperature water for 6 min. A video

camera was used to record activity from the side. Time spent immobile was scored for the final 5 min of the trial.

Neuropathology

Mice were anesthetized with 2.5% Avertin IP followed by transcardiac perfusion with PBS and 4% PFA. Brains were postfixed in 4% PFA in PBS for 24 h at 4°C. Brains were cryoprotected in 30% sucrose with 0.01% sodium azide. Once equilibrated, brains were divided into forebrain and cerebellum and weighed. Forebrains were then frozen on dry ice, mounted in Tissue-TEK O.C.T. embedding compound (Sakura) and cut via cryostat (Leica CM3050S) into a series of 25 μm coronal sections free-floating in PBS with 0.01% sodium azide.

Stereological volumetric analysis was performed as previously described (72). Briefly, a series of sections spaced 200 μm apart and spanning the striatum were stained for NeuN (1:1000, Millipore) using biotinylated anti-mouse secondary antibody (1:1000, Vector Laboratories), the ABC Elite Kit (Vector) to amplify signal and 3, 3′-diaminobenzidine (Thermo Scientific) detection. Structures were traced using Stereo Investigator software (MBF Bioscience) and volumes determined using the Cavalieri principle.

Quantification of GFAP staining

GFAP immunostaining and imaging were performed as previously described (73) using a series of four sections spaced 200 μm apart and spanning the central portion of the striatum. Quantification of GFAP staining was performed using ImageJ software. The striatum was traced, and the region of interest (ROI) obtained. The threshold was set by adjusting the upper bar to visualize GFAP staining while maintaining a dark background. The lower bar was kept at a value of 255. Threshold settings were maintained for image stacks of all sections from each brain and all brains of each cohort. The integrated optical density of staining was measured using the ROI manager and the average value for each mouse was used for analysis.

Statistical analysis

Mice exhibiting a reactive phenotype as determined by abnormal brain morphology (enlarged triangular forebrain and total brain weight over 500 mg) were excluded from behavioral analysis. Data are expressed as mean ± S.E.M. unless otherwise noted. Analyses were performed with one- or two-way-ANOVA and Bonferroni *post hoc* tests (significance markers on figures) using GraphPad Prism 5.0 unless otherwise noted. Differences were considered statistically significant for $P < 0.05$.

Supplementary Material

Supplementary Material is available at *HMG* online.

Acknowledgements

A.L.S. held postdoctoral fellowships from the CIHR, The Huntington Society of Canada, the Michael Smith Foundation for Health Research and The Huntington's Disease Society of America. The authors thank Mahsa Amirabbasi, Mark Wang, Sheng Yu and Qingwen Xia for their technical support.

Conflict of Interest statement. M.R.H. is an employee of Teva Pharmaceuticals, Inc. Teva supported portions of this study but did not play a role in the design, analysis or interpretation of this study. All other authors declare no competing financial interests.

Funding

This work was supported by the Canadian Institutes of Health Research (CIHR), grant number 20R90174, and a sponsored research agreement with Teva Pharmaceuticals.

References

1. Chakraborty, J., Rajamma, U. and Mohanakumar, K.P. (2014) A mitochondrial basis for Huntington's disease: therapeutic prospects. *Mol. Cell. Biochem.*, **389**, 277–291.
2. Johri, A. and Beal, M.F. (2012) Antioxidants in Huntington's disease. *Biochim. Biophys. Acta*, **1822**, 664–674.
3. Sepers, M.D. and Raymond, L.A. (2014) Mechanisms of synaptic dysfunction and excitotoxicity in Huntington's disease. *Drug Discov. Today*, **19**, 990–996.
4. Valencia, A., Sapp, E., Kimm, J.S., McClory, H., Reeves, P.B., Alexander, J., Ansong, K.A., Masso, N., Frosch, M.P., Kegel, K.B. *et al.* (2013) Elevated NADPH oxidase activity contributes to oxidative stress and cell death in Huntington's disease. *Hum. Mol. Genet.*, **22**, 1112–1131.
5. Zuccato, C. and Cattaneo, E. (2014) Huntington's disease. *Handb. Exp. Pharmacol.*, **220**, 357–409.
6. Beal, M.F., Brouillet, E., Jenkins, B., Henshaw, R., Rosen, B. and Hyman, B.T. (1993) Age-dependent striatal excitotoxic lesions produced by the endogenous mitochondrial inhibitor malonate. *J. Neurochem.*, **61**, 1147–1150.
7. Brouillet, E., Jenkins, B.G., Hyman, B.T., Ferrante, R.J., Kowall, N.W., Srivastava, R., Roy, D.S., Rosen, B.R. and Beal, M.F. (1993) Age-dependent vulnerability of the striatum to the mitochondrial toxin 3-nitropropionic acid. *J. Neurochem.*, **60**, 356–359.
8. Song, W., Chen, J., Petrilli, A., Liot, G., Klinglmayr, E., Zhou, Y., Poquiz, P., Tjong, J., Pouladi, M.A., Hayden, M.R. *et al.* (2011) Mutant huntingtin binds the mitochondrial fission GTPase dynamin-related protein-1 and increases its enzymatic activity. *Nat. Med.*, **17**, 377–382.
9. Trushina, E., Dyer, R.B., Badger, J.D., II, Ure, D., Eide, L., Tran, D.D., Vrieze, B.T., Legendre-Guillemin, V., McPherson, P.S., Mandavilli, B.S. *et al.* (2004) Mutant huntingtin impairs axonal trafficking in mammalian neurons in vivo and in vitro. *Mol. Cell. Biol.* **24**, 8195–8209.
10. Wong, Y.C. and Holzbaur, E.L. (2014) The regulation of autophagosome dynamics by huntingtin and HAP1 is disrupted by expression of mutant huntingtin, leading to defective cargo degradation. *J. Neurosci.*, **34**, 1293–1305.
11. Yano, H., Baranov, S.V., Baranova, O.V., Kim, J., Pan, Y., Yablonska, S., Carlisle, D.L., Ferrante, R.J., Kim, A.H. and Friedlander, R.M. (2014) Inhibition of mitochondrial protein import by mutant huntingtin. *Nat. Neurosci.*, **17**, 822–831.
12. Klepac, N., Relja, M., Klepac, R., Hecimovic, S., Babic, T. and Trkulja, V. (2007) Oxidative stress parameters in plasma of Huntington's disease patients, asymptomatic Huntington's disease gene carriers and healthy subjects: a cross-sectional study. *J. Neurol.*, **254**, 1676–1683.
13. Sorolla, M.A., Reverter-Branchat, G., Tamarit, J., Ferrer, I., Ros, J. and Cabiscol, E. (2008) Proteomic and oxidative stress

analysis in human brain samples of Huntington disease. *Free Radic. Biol. Med.*, **45**, 667–678.
14. Kim, J., Moody, J.P., Edgerly, C.K., Bordiuk, O.L., Cormier, K., Smith, K., Beal, M.F. and Ferrante, R.J. (2010) Mitochondrial loss, dysfunction and altered dynamics in Huntington's disease. *Hum. Mol. Genet.*, **19**, 3919–3935.
15. Rotblat, B., Southwell, A.L., Ehrnhoefer, D.E., Skotte, N.H., Metzler, M., Franciosi, S., Leprivier, G., Somasekharan, S.P., Barokas, A., Deng, Y. *et al.* (2014) hace1 reduces oxidative stress and mutant Huntingtin toxicity by promoting the NRF2 response. *Proc. Natl. Acad. Sci. U. S. A.*, **111**, 3032–3037.
16. Sykiotis, G.P. and Bohmann, D. (2010) Stress-activated cap'n'collar transcription factors in aging and human disease. *Sci. Signal.*, **3**, re3.
17. Slow, E.J., van Raamsdonk, J., Rogers, D., Coleman, S.H., Graham, R.K., Deng, Y., Oh, R., Bissada, N., Hossain, S.M., Yang, Y.-Z. *et al.* (2003) Selective striatal neuronal loss in a YAC128 mouse model of Huntington disease. *Hum. Mol. Genet.*, **12**, 1555–1567.
18. Pouladi, M.A., Morton, A.J. and Hayden, M.R. (2013) Choosing an animal model for the study of Huntington's disease. *Nat. Rev. Neurosci.*, **14**, 708–721.
19. Brocardo, P.S., McGinnis, E., Christie, B.R. and Gil-Mohapel, J. (2016) Time-course analysis of protein and lipid oxidation in the brains of Yac128 Huntington's disease transgenic mice. *Rejuvenation Res.*, **19**, 140–148.
20. Gan, L. and Johnson, J.A. (2014) Oxidative damage and the Nrf2-ARE pathway in neurodegenerative diseases. *Biochim. Biophys. Acta*, **1842**, 1208–1218.
21. Bell, K.F., Al-Mubarak, B., Martel, M.A., McKay, S., Wheelan, N., Hasel, P., Markus, N.M., Baxter, P., Deighton, R.F., Serio, A. *et al.* (2015) Neuronal development is promoted by weakened intrinsic antioxidant defences due to epigenetic repression of Nrf2. *Nat. Commun.*, **6**, 7066.
22. Yu, X., Song, N., Guo, X., Jiang, H., Zhang, H. and Xie, J. (2016) Differences in vulnerability of neurons and astrocytes to heme oxygenase-1 modulation: implications for mitochondrial ferritin. *Sci. Rep.*, **6**, 24200.
23. Li, J., Johnson, D., Calkins, M., Wright, L., Svendsen, C. and Johnson, J. (2005) Stabilization of Nrf2 by tBHQ confers protection against oxidative stress-induced cell death in human neural stem cells. *Toxicol. Sci.*, **83**, 313–328.
24. Dinkova-Kostova, A.T. and Abramov, A.Y. (2015) The emerging role of Nrf2 in mitochondrial function. *Free Radic. Biol. Med.*, **88**, 179–188.
25. Brand, M.D. and Nicholls, D.G. (2011) Assessing mitochondrial dysfunction in cells. *Biochem. J.*, **435**, 297–312.
26. Divakaruni, A.S., Paradyse, A., Ferrick, D.A., Murphy, A.N. and Jastroch, M. (2014) Analysis and interpretation of microplate-based oxygen consumption and pH data. *Methods Enzymol.*, **547**, 309–354.
27. Holmstrom, K.M., Baird, L., Zhang, Y., Hargreaves, I., Chalasani, A., Land, J.M., Stanyer, L., Yamamoto, M., Dinkova-Kostova, A.T. and Abramov, A.Y. (2013) Nrf2 impacts cellular bioenergetics by controlling substrate availability for mitochondrial respiration. *Biol. Open*, **2**, 761–770.
28. Chiu, S.-C., Lin, Y.-J., Huang, S.-Y., Lien, C.-F., Chen, S.-P., Pang, C.-Y., Lin, J.-H., Yang, K.-T. and Gallyas, F. (2015) The role of intermittent hypoxia on the proliferative inhibition of rat cerebellar astrocytes. *PLoS One*, **10**, e0132263.
29. Choi, I., Choi, D.-J., Yang, H., Woo, J.H., Chang, M.-Y., Kim, J.Y., Sun, W., Park, S.-M., Jou, I., Lee, S.-H. and Joe, E.-H. (2016) PINK1 expression increases during brain development and stem cell differentiation, and affects the development of GFAP-positive astrocytes. *Mol. Brain*, **9**, 5.
30. Choi, I., Kim, J., Jeong, H.K., Kim, B., Jou, I., Park, S.M., Chen, L., Kang, U.J., Zhuang, X. and Joe, E.H. (2013) PINK1 deficiency attenuates astrocyte proliferation through mitochondrial dysfunction, reduced AKT and increased p38 MAPK activation, and downregulation of EGFR. *Glia*, **61**, 800–812.
31. Ghosh, R. and Tabrizi, S. (2013) Clinical Aspects of Huntington's Disease. In Nguyen, H.H.P. and Cenci, M. A. (eds.) *Behavioural Neurobiology of Huntington's Disease and Parkinson's Disease*, Current Topics in Behavioral Neurosciences 22. Springer-Verlag Berlin Heidelberg, Germany, pp. 1–29.
32. Van Raamsdonk, J.M., Pearson, J., Slow, E.J., Hossain, S.M., Leavitt, B.R. and Hayden, M.R. (2005) Cognitive dysfunction precedes neuropathology and motor abnormalities in the YAC128 mouse model of Huntington's disease. *J. Neurosci.*, **25**, 4169–4180.
33. Southwell, A.L., Ko, J. and Patterson, P.H. (2009) Intrabody gene therapy ameliorates motor, cognitive, and neuropathological symptoms in multiple mouse models of Huntington's disease. *J. Neurosci.*, **29**, 13589–13602.
34. Southwell, A.L., Franciosi, S., Villanueva, E.B., Xie, Y., Winter, L.A., Veeraraghavan, J., Jonason, A., Felczak, B., Zhang, W., Kovalik, V. *et al.* (2015) Anti-semaphorin 4D immunotherapy ameliorates neuropathology and some cognitive impairment in the YAC128 mouse model of Huntington disease. *Neurobiol. Dis.*, **76**, 46–56.
35. Pouladi, M.A., Graham, R.K., Karasinska, J.M., Xie, Y., Santos, R.D., Petersen, A. and Hayden, M.R. (2008) Prevention of depressive behaviour in the YAC128 mouse model of Huntington disease by mutation at residue 586 of huntingtin. *Brain*, **132**, 919–932.
36. Pouladi, M.A., Stanek, L.M., Xie, Y., Franciosi, S., Southwell, A.L., Deng, Y., Butland, S., Zhang, W., Cheng, S.H., Shihabuddin, L.S. *et al.* (2012) Marked differences in neurochemistry and aggregates despite similar behavioural and neuropathological features of Huntington disease in the full-length BACHD and YAC128 mice. *Hum. Mol. Genet.*, **21**, 2219–2232.
37. Vonsattel, J. (2008) Huntington disease models and human neuropathology: similarities and differences. *Acta Neuropathol.*, **115**, 55–69.
38. Bayram-Weston, Z., Jones, L., Dunnett, S.B. and Brooks, S.P. (2012) Light and electron microscopic characterization of the evolution of cellular pathology in YAC128 Huntington's disease transgenic mice. *Brain Res. Bull.*, **88**, 137–147.
39. Van Raamsdonk, J.M., Metzler, M., Slow, E., Pearson, J., Schwab, C., Carroll, J., Graham, R.K., Leavitt, B.R. and Hayden, M.R. (2007) Phenotypic abnormalities in the YAC128 mouse model of Huntington disease are penetrant on multiple genetic backgrounds and modulated by strain. *Neurobiol. Dis.*, **26**, 189–200.
40. Schauwecker, P.E. and Steward, O. (1997) Genetic determinants of susceptibility to excitotoxic cell death: implications for gene targeting approaches. *Proc. Natl. Acad. Sci. U. S. A.*, **94**, 4103–4108.
41. Gogliotti, R.G., Lutz, C., Jorgensen, M., Huebsch, K., Koh, S. and DiDonato, C.J. (2011) Characterization of a commonly used mouse model of SMA reveals increased seizure susceptibility and heightened fear response in FVB/N mice. *Neurobiol. Dis.*, **43**, 142–151.

42. Goelz, M.F., Mahler, J., Harry, J., Myers, P., Clark, J., Thigpen, J.E. and Forsythe, D.B. (1998) Neuropathologic findings associated with seizures in FVB mice. *Lab. Anim. Sci.*, **48**, 34–37.
43. Hsiao, K.K., Borchelt, D.R., Olson, K., Johannsdottir, R., Kitt, C., Yunis, W., Xu, S., Eckman, C., Younkin, S., Price, D. *et al.* (1995) Age-related CNS disorder and early death in transgenic FVB/N mice overexpressing Alzheimer amyloid precursor proteins. *Neuron*, **15**, 1203–1218.
44. Nichols, N.R., Day, J.R., Laping, N.J., Johnson, S.A. and Finch, C.E. (1993) GFAP mRNA increases with age in rat and human brain. *Neurobiol. Aging*, **14**, 421–429.
45. Goss, J.R., Finch, C.E. and Morgan, D.G. (1991) Age-related changes in glial fibrillary acidic protein mRNA in the mouse brain. *Neurobiol. Aging*, **12**, 165–170.
46. Hubbs, A.F., Benkovic, S.A., Miller, D.B., O'Callaghan, J.P., Battelli, L., Schwegler-Berry, D. and Ma, Q. (2007) Vacuolar leukoencephalopathy with widespread astrogliosis in mice lacking transcription factor Nrf2. *Am. J. Pathol.*, **170**, 2068–2076.
47. Mason, R.P., Casu, M., Butler, N., Breda, C., Campesan, S., Clapp, J., Green, E.W., Dhulkhed, D., Kyriacou, C.P. and Giorgini, F. (2013) Glutathione peroxidase activity is neuroprotective in models of Huntington's disease. *Nat. Genet.*, **45**, 1249–1254.
48. Shirendeb, U.P., Calkins, M.J., Manczak, M., Anekonda, V., Dufour, B., McBride, J.L., Mao, P. and Reddy, P.H. (2012) Mutant huntingtin's interaction with mitochondrial protein Drp1 impairs mitochondrial biogenesis and causes defective axonal transport and synaptic degeneration in Huntington's disease. *Hum. Mol. Genet.*, **21**, 406–420.
49. Chaturvedi, R.K., Calingasan, N.Y., Yang, L., Hennessey, T., Johri, A. and Beal, M.F. (2010) Impairment of PGC-1alpha expression, neuropathology and hepatic steatosis in a transgenic mouse model of Huntington's disease following chronic energy deprivation. *Hum. Mol. Genet.*, **19**, 3190–3205.
50. Cui, L., Jeong, H., Borovecki, F., Parkhurst, C.N., Tanese, N. and Krainc, D. (2006) Transcriptional repression of PGC-1alpha by mutant huntingtin leads to mitochondrial dysfunction and neurodegeneration. *Cell*, **127**, 59–69.
51. Taherzadeh-Fard, E., Saft, C., Andrich, J., Wieczorek, S. and Arning, L. (2009) PGC-1alpha as modifier of onset age in Huntington disease. *Mol. Neurodegener.*, **4**, 10.
52. Tsunemi, T., Ashe, T.D., Morrison, B.E., Soriano, K.R., Au, J., Roque, R.A., Lazarowski, E.R., Damian, V.A., Masliah, E. and La Spada, A.R. (2012) PGC-1alpha rescues Huntington's disease proteotoxicity by preventing oxidative stress and promoting TFEB function. *Sci. Transl. Med.*, **4**, 142ra197.
53. Weydt, P., Pineda, V.V., Torrence, A.E., Libby, R.T., Satterfield, T.F., Lazarowski, E.R., Gilbert, M.L., Morton, G.J., Bammler, T.K., Strand, A.D. *et al.* (2006) Thermoregulatory and metabolic defects in Huntington's disease transgenic mice implicate PGC-1alpha in Huntington's disease neurodegeneration. *Cell Metab.*, **4**, 349–362.
54. Weydt, P., Soyal, S.M., Gellera, C., Didonato, S., Weidinger, C., Oberkofler, H., Landwehrmeyer, G.B. and Patsch, W. (2009) The gene coding for PGC-1alpha modifies age at onset in Huntington's disease. *Mol. Neurodegener.*, **4**, 3.
55. Lin, J., Handschin, C. and Spiegelman, B.M. (2005) Metabolic control through the PGC-1 family of transcription coactivators. *Cell Metab.*, **1**, 361–370.
56. Marmolino, D., Manto, M., Acquaviva, F., Vergara, P., Ravella, A., Monticelli, A., Pandolfo, M. and Andreu, A.L. (2010) PGC-1alpha down-regulation affects the antioxidant response in Friedreich's ataxia. *PLoS One*, **5**, e10025.
57. Ellrichmann, G., Petrasch-Parwez, E., Lee, D.H., Reick, C., Arning, L., Saft, C., Gold, R. and Linker, R.A. (2011) Efficacy of fumaric acid esters in the R6/2 and YAC128 models of Huntington's disease. *PLoS One*, **6**, e16172.
58. Stack, C., Ho, D., Wille, E., Calingasan, N.Y., Williams, C., Liby, K., Sporn, M., Dumont, M. and Beal, M.F. (2010) Triterpenoids CDDO-ethyl amide and CDDO-trifluoroethyl amide improve the behavioral phenotype and brain pathology in a transgenic mouse model of Huntington's disease. *Free Radic. Biol. Med.*, **49**, 147–158.
59. Calkins, M.J., Jakel, R.J., Johnson, D.A., Chan, K., Kan, Y.W. and Johnson, J.A. (2005) Protection from mitochondrial complex II inhibition in vitro and in vivo by Nrf2-mediated transcription. *Proc. Natl. Acad. Sci. U. S. A.*, **102**, 244–249.
60. Boussicault, L., Herard, A.S., Calingasan, N., Petit, F., Malgorn, C., Merienne, N., Jan, C., Gaillard, M.C., Lerchundi, R. and Barros, L.F. (2014) Impaired brain energy metabolism in the BACHD mouse model of Huntington's disease: critical role of astrocyte-neuron interactions. *J. Cereb. Blood Flow Metab.*, **34**, 1500–1510.
61. Lee, W., Reyes, R.C., Gottipati, M.K., Lewis, K., Lesort, M., Parpura, V. and Gray, M. (2013) Enhanced Ca(2+)-dependent glutamate release from astrocytes of the BACHD Huntington's disease mouse model. *Neurobiol. Dis.*, **58**, 192–199.
62. Benraiss, A., Wang, S., Herrlinger, S., Li, X., Chandler-Militello, D., Mauceri, J., Burm, H.B., Toner, M., Osipovitch, M., Jim Xu, Q. *et al.* (2016) Human glia can both induce and rescue aspects of disease phenotype in Huntington disease. *Nat. Commun.*, **7**, 11758.
63. Bal-Price, A. and Brown, G.C. (2001) Inflammatory neurodegeneration mediated by nitric oxide from activated glia-inhibiting neuronal respiration, causing glutamate release and excitotoxicity. *J. Neurosci.*, **21**, 6480–6491.
64. Ehrnhoefer, D.E., Butland, S.L., Pouladi, M.A. and Hayden, M.R. (2009) Mouse models of Huntington disease: variations on a theme. *Dis. Model. Mech.*, **2**, 123–129.
65. Zhang, L., Anglesio, M.S., O'Sullivan, M., Zhang, F., Yang, G., Sarao, R., Nghiem, M.P., Cronin, S., Hara, H., Melnyk, N. *et al.* (2007) The E3 ligase hace1 is a critical chromosome 6q21 tumor suppressor involved in multiple cancers. *Nat. Med.*, **13**, 1060–1069.
66. Leavitt, B.R., van Raamsdonk, J.M., Shehadeh, J., Fernandes, H., Murphy, Z., Graham, R.K., Wellington, C.L., Raymond, L.A. and Hayden, M.R. (2006) Wild-type huntingtin protects neurons from excitotoxicity. *J. Neurochem.*, **96**, 1121–1129.
67. Graham, R.K., Deng, Y., Slow, E.J., Haigh, B., Bissada, N., Lu, G., Pearson, J., Shehadeh, J., Bertram, L., Murphy, Z. *et al.* (2006) Cleavage at the caspase-6 site is required for neuronal dysfunction and degeneration due to mutant huntingtin. *Cell*, **125**, 1179–1191.
68. Metzler, M., Gan, L., Mazarei, G., Graham, R.K., Liu, L., Bissada, N., Lu, G., Leavitt, B.R. and Hayden, M.R. (2010) Phosphorylation of huntingtin at Ser421 in YAC128 neurons is associated with protection of YAC128 neurons from NMDA-mediated excitotoxicity and is modulated by PP1 and PP2A. *J. Neurosci.*, **30**, 14318–14329.
69. Van Raamsdonk, J.M., Pearson, J., Rogers, D.A., Bissada, N., Vogl, A.W., Hayden, M.R. and Leavitt, B.R. (2005) Loss of wild-type huntingtin influences motor dysfunction and survival in the YAC128 mouse model of Huntington disease. *Hum. Mol. Genet.*, **14**, 1379–1392.
70. Hodgson, J.G., Smith, D.J., McCutcheon, K., Koide, H.B., Nishiyama, K., Dinulos, M.B., Stevens, M.E., Bissada, N.,

Nasir, J., Kanazawa, I. *et al*. (1996) Human huntingtin derived from YAC transgenes compensates for loss of murine huntingtin by rescue of the embryonic lethal phenotype. *Hum. Mol. Genet*., **5**, 1875–1885.

71. Skotte, N.H., Southwell, A.L., Ostergaard, M.E., Carroll, J.B., Warby, S.C., Doty, C.N., Petoukhov, E., Vaid, K., Kordasiewicz, H., Watt, A.T. *et al*. (2014) Allele-specific suppression of mutant huntingtin using antisense oligonucleotides: providing a therapeutic option for all Huntington disease patients. *PLoS One*, **9**, e107434.
72. Southwell, A.L., Warby, S.C., Carroll, J.B., Doty, C.N., Skotte, N.H., Zhang, W., Villanueva, E.B., Kovalik, V., Xie, Y., Pouladi, M.A. *et al*. (2013) A fully humanized transgenic mouse model of Huntington disease. *Hum. Mol. Genet*., **22**, 18–34.
73. Southwell, A.L., Skotte, N.H., Kordasiewicz, H.B., Ostergaard, M.E., Watt, A.T., Carroll, J.B., Doty, C.N., Villanueva, E.B., Petoukhov, E., Vaid, K. *et al*. (2014) In vivo evaluation of candidate allele-specific mutant huntingtin gene silencing antisense oligonucleotides. *Mol. Ther*., **22**, 2093–2106.